

Effects of cryoprotectant concentration and cooling rate on vitrification of aqueous solutions

Viatcheslav Berejnov, Naji S. Hussein, Osama A. Alsaied and Robert E. Thorne

Copyright © International Union of Crystallography

Author(s) of this paper may load this reprint on their own web site provided that this cover page is retained. Reproduction of this article or its storage in electronic databases or the like is not permitted without prior permission in writing from the IUCr.

Effects of cryoprotectant concentration and cooling rate on vitrification of aqueous solutions

Viatcheslav Berejnov,^{a*} Naji S. Hussein,^b Osama A. Alsaied^c and Robert E. Thorne^a^aPhysics Department, Cornell University, USA, ^bApplied and Engineering Physics Department, Cornell University, USA, and ^cWeill Cornell Medical College, Doha, Qatar.

Correspondence e-mail: vb54@cornell.edu

Vitrification of aqueous cryoprotectant mixtures is essential in cryopreservation of proteins and other biological samples. Systematic measurements of critical cryoprotective agent (CPA) concentrations required for vitrification during plunge-cooling from $T = 295$ K to $T = 77$ K in liquid nitrogen are reported. Measurements on fourteen common CPAs, including alcohols (glycerol, methanol, 2-propanol), sugars (sucrose, xylitol, dextrose, trehalose), polyethylene glycols (ethylene glycol, PEG 200, PEG 2000, PEG 20000), glycols [dimethyl sulfoxide (DMSO), 2-methyl-2,4-pentanediol (MPD)], and salt (NaCl), were performed for volumes ranging over four orders of magnitude from ~ 1 nl to $20 \mu\text{l}$, and covering the range of interest in protein crystallography. X-ray diffraction measurements on aqueous glycerol mixtures confirm that the polycrystalline-to-vitreous transition occurs within a span of less than 2% *w/v* in CPA concentration, and that the form of polycrystalline ice (hexagonal or cubic) depends on CPA concentration and cooling rate. For most of the studied cryoprotectants, the critical concentration decreases strongly with volume in the range from $\sim 5 \mu\text{l}$ to $\sim 0.1 \mu\text{l}$, typically by a factor of two. By combining measurements of the critical concentration *versus* volume with cooling time *versus* volume, the function of greatest intrinsic physical interest is obtained: the critical CPA concentration *versus* cooling rate during flash-cooling. These results provide a basis for more rational design of cryoprotective protocols, and should yield insight into the physics of glass formation in aqueous mixtures.

© 2006 International Union of Crystallography
Printed in Great Britain – all rights reserved

1. Introduction

Cryocrystallographic methods play a central role in protein crystallography (Hope, 1990; Rodgers, 1994; Chayen *et al.*, 1996; Garman & Schneider, 1997; Garman, 1999; Juers & Matthews, 2004). The amount of data that can be collected from a crystal before significant degradation in the X-ray beam occurs is increased and, compared with room-temperature data collection in glass capillaries, crystal handling is in many ways simplified. These large benefits have accrued even though many aspects of the cryoprotection and flash-cooling processes have been poorly understood.

Protein crystals are mechanically very fragile. Because they contain (and can be surrounded by) large amounts of water, formation and growth of water ice crystals during cooling degrades protein crystal order and diffraction properties (Garman & Schneider, 1997). Instead, water must be cooled into an amorphous, vitreous or glassy state in which the liquid phase's lack of long-range order is preserved, but its molecular motions are frozen out.

Glass formation during cooling occurs only if crystal nucleation is somehow suppressed. Because of thermo-

dynamic and kinetic barriers, formation of crystal nuclei requires a finite time, so higher cooling rates reduce the probability of nucleation and favor glass formation. The nucleation probability also depends on how liquid properties like viscosity vary with temperature, and thus on the detailed form of the cooling path $T(t)$. Cryoprotective agents (CPAs) like glycerol, which dissolve in or fully mix with water, modify molecular diffusion relevant to nucleation. However, they can also lead to changes in protein structure and, if introduced *via* post-growth soaks, can cause osmotic shock and crystal damage, especially at higher concentrations. The vitreous ice/polycrystalline ice phase diagram as a function of cryoprotectant concentration thus provides an important tool for optimizing cryopreservation protocols.

The conventional method used to determine vitreous/crystal phase diagrams in the temperature/concentration plane is based on differential scanning calorimetry (DSC) (MacKenzie, 1977). A metal or glass container holding a solution volume of ~ 10 – $100 \mu\text{l}$ is plunged into liquid nitrogen to cool the solution into the vitreous state. Typical cooling rates in DSC experiments are $<10 \text{ K s}^{-1}$, and the cooling history determines the properties of the glassy state. Calorimetry

measurements are then performed as the sample is warmed, typically at $\sim 1 \text{ K s}^{-1}$. For the slow cooling rates typical of DSC, homogeneous crystal nucleation occurs below a critical CPA concentration C_m (Luyet & Rasmussen, 1968; Rasmussen & Luyet, 1970; Fahy *et al.*, 1984). Above C_m , only heterogeneous nucleation occurs, and this can be suppressed either by using 'clean' samples or by reducing the sample size. Homogeneous and heterogeneous nucleation can be distinguished by comparing the behavior of bulk liquid, thin films (Turnbull & Fisher, 1949) and emulsions (Luyet & Rasmussen, 1968; Rasmussen & Luyet, 1970). C_m thus determines the minimum CPA concentration required to achieve vitrified ice under slow-cooling conditions. In protein crystallography, sample volumes range from microlitres to picolitres, which is orders of magnitude smaller than in DSC measurements. The cooling rates are therefore much larger, so the CPA concentrations needed to achieve vitreous ice should be smaller.

To date, the kinetic phase diagrams giving the minimum (critical) CPA concentration required for vitrification during plunge-cooling in common liquid cryogenes have not been determined for any CPA in the volume/cooling rate range relevant to cryocrystallography. In particular, the development of microfabricated mounts (Thorne *et al.*, 2003) as a replacement for loops in cryocrystallography has allowed very small crystals to be routinely mounted with very little surrounding liquid, and there is no information on CPA concentrations required for vitrification in such small volumes. Recent experiments (Garman & Mitchell, 1996; McFerrin & Snell, 2002; Chinte *et al.*, 2005) have probed the behavior of larger volumes obtained by mixing glycerol with Hampton crystallization screens, with 5% *v/v* glycerol concentration increments. These screens contain multiple components, such

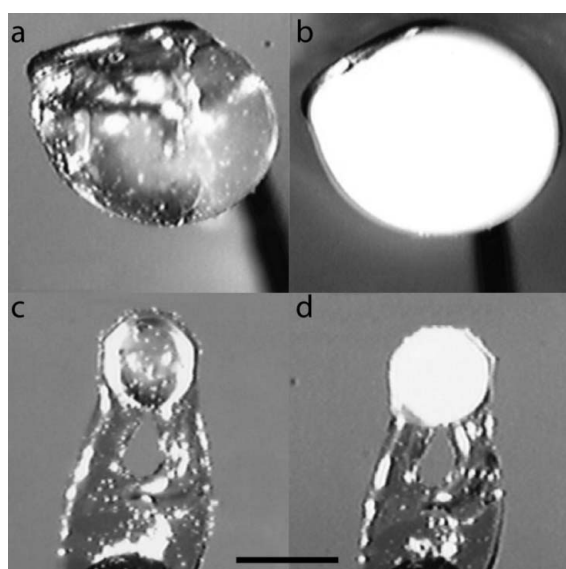


Figure 1
Flash-cooled glycerol solutions above and below the critical concentration for vitrification. (a) 500 nl of 42% *w/v* glycerol on a tungsten loop; (b) 500 nl of 38% *w/v* glycerol on a tungsten loop; (c) 50 nl of 30% *w/v* glycerol on a 500 μm MicroMount; (d) 50 nl of 26% *w/v* glycerol on a 500 μm MicroMount. The critical concentrations for 500 nl and 50 nl are 40% *w/v* and 28% *w/v*, respectively. The bar represents 500 μm .

as salts and other CPAs, and the liquid volumes have not been accurately measured, making detailed interpretation of results difficult. Critical CPA concentrations are of interest not just in protein crystallography but more generally in cryopreservation of biological samples. This suggests binary aqueous solutions as the starting point for systematic study.

We have determined the vitreous ice/polycrystalline ice phase diagrams of CPA concentration *versus* volume for plunge-cooling in liquid nitrogen. We have examined volumes varying by up to five orders of magnitude, from $\sim 1 \text{ nl}$ (0.1 nl for glycerol) to 20 μl . The measurements were made for fourteen different penetrating and nonpenetrating cryoprotectants, including alcohols (glycerol, methanol, 2-propanol), sugars (sucrose, xylitol, dextrose, trehalose), polyethylene glycols (PEGs) (ethylene glycol, PEG 200, PEG 2000, PEG 20000), glycols [dimethyl sulfoxide (DMSO), 2-methyl-2,4-pentanediol (MPD)], and salt (NaCl). Drops of solution were plunge-cooled from $T = 295 \text{ K}$ into liquid nitrogen at $T = 77 \text{ K}$. The resulting low-temperature phase, vitreous or polycrystalline, was determined from visual observation of whether the drops remained transparent or became opaque, supplemented by X-ray diffraction measurements. For the most common CPAs, the required concentration is a strong function of volume, and for typical volumes relevant in protein crystallography, it is roughly half that required for volumes greater than 10 μl . For glycerol, we have also determined the critical concentration for vitrification *versus* cooling rate.

2. Materials and methods

2.1. Preparation of CPA solutions

All cryoprotective agents were obtained from Sigma-Aldrich (St Louis, MO, USA). CPAs were mixed with distilled deionized (DI) water to produce aliquots in increments of 2% weight per volume (*w/v*). For solid CPAs, weighing errors were less than 1%. For liquid CPAs, uncertainties in dilution with DI water in volumetric flasks were less than 1%. To ensure full mixing for solid CPAs near their solubility limits and for high-viscosity liquid CPAs, the solutions were heated, stirred and sonicated.

2.2. Drop dispensing, holding and volume estimation

Four types of sample holder were used to accommodate different sample volumes: (1) 24 gauge (0.51 mm diameter) copper loops with 1.6–1.7 mm diameters and (2) 36 gauge (0.13 mm diameter) tungsten loops with $\sim 0.9 \text{ mm}$ diameters were used for volumes of 7.5 μl to 20 μl and 100 nl to 7.5 μl , respectively; (3) MicroMounts (Mitegen, Ithaca, NY, USA) made from 10 μm polyimide films with apertures of 100 to 500 μm were used for volumes smaller than 100 nl; and (4) CryoLoops (Hampton Research, Laguna Niguel, CA, USA) of 10 μm nylon with nominal apertures of 0.1–0.5 mm were used for volumes between 200 and 100 nl. In all cases, experiments were performed to verify that the sample holder did not limit cooling rates.

Table 1

Typical volumes V , aspect ratios R , relative volume errors (%), dispensers (a : Pipetman P20, b : Pipetman P2) and sample holders (1: copper loop, 2: tungsten loop, and 3: MicroMount, with aperture in μm , as described in the text) for the aqueous CPA samples used in these experiments.

V (μl)	R	Relative error %, dispenser			Holder
20	>0.8	0.5	a		1
15	>0.8	1.5	a		1
10	>0.8	0.5	a		1
7.5	>0.8	1.4	a		1
5.0	>0.8	2.4	a		1
2.0	>0.8	6.3	a	2.2	2
1.5	>0.8	5.6	a	5.6	2
1.0	>0.8	16	a	11	2
0.5	0.8			24	2
0.4	1.0			29	2
0.3	0.9			36	2
0.2	0.8			49	2
0.1†	0.6			77	2
0.050	0.4			5	3, 500 μm
0.025	0.3			7	3, 400 μm
0.010	0.4			8	3, 300 μm
0.005	0.4			12	3, 200 μm
0.0002	0.3			36	3,‡ 100 μm

† 0.5 mm CryoLoop used for X-ray data collection. ‡ 100 μm MicroMount used for X-ray data collection.

Larger-volume drops were dispensed onto the metal loops using a pipette (P2 and P20, Gilson, Pipetman, Middleton, WI, USA). As shown in Figs. 1(a) and 1(b), the resulting drops were nearly spherical with very little liquid–metal contact, and had radii slightly larger than the loop radii. Small-volume drops were prepared by immersing CryoLoops or MicroMounts directly into CPA solutions. CryoLoops yielded nearly spherical drops. The smallest drops prepared using MicroMounts were flattened in the plane of the circular aperture, with aspect ratios of roughly 0.3–0.4. To determine drop volumes captured by CryoLoops and MicroMounts, the drops were treated as oblate spheroids, and the dimensions of their axes measured using a microscope. The volume was calculated as $V = (4/3)\pi x^2 z$, where x is the radius in the plane of the aperture and z is half of the drop’s height. The error in the volume was calculated using standard error propagation based on the error in the dimensions of the drops. Table 1 shows typical measured drop dimensions and calculated volumes.

2.3. Cooling and visual phase inspection

Flash-cooling was performed by immersing samples in liquid nitrogen (LN_2) contained in a glass hemispherical Dewar (# 8130, Pope Scientific Inc, Saukville, WI, USA). In some experiments, the nitrogen was cooled below its boiling point by reducing the pressure above the LN_2 /vapor interface. The Dewar was sealed with an O-ring by a transparent, 1 cm thick Plexiglass lid, and connected to a vacuum pressure station equipped with a pressure gauge (Barnat). After pumping, boiling in the open Dewar was eliminated. However, no appreciable difference in flash-cooling results for boiling ($T = 77\text{ K}$) and cooled LN_2 was observed, so most data were collected at $T = 77\text{ K}$.

Drops were plunged by hand from room temperature ($T = 295\text{ K}$) into LN_2 within a second after mounting, to prevent

any condensation or evaporation that could change the sample composition and volume. The plunge depth was $\sim 1\text{--}2\text{ cm}$ below the LN_2 surface and the plunge speed was $\sim 10\text{ cm s}^{-1}$. To maximize heat transfer, drops were agitated at $\sim 1\text{ cm s}^{-1}$ for several seconds until all boiling had ceased. The boiling time for drop plus holder ranged from a few seconds for the largest drops in copper wire holders to a time shorter than could be resolved by eye for the smallest drops in MicroMounts. Initially, boiling involved nearly periodic evolution of single bubbles, 2–3 mm in diameter. These bubbles were much larger than the drop size and formed a film around the drop during their growth. We identify this as the film-boiling regime (Incropera & DeWitt, 1981; van Stralen & Cole, 1979). Boiling behavior then showed an abrupt and visually obvious transition to simultaneous evolution of several small bubbles with sizes much smaller than the drop size, which we identify as the bubble-nucleation regime. Each region produces characteristic sounds as the bubbles break the LN_2 surface, and the transition between them can easily be heard. For larger drop volumes ($>0.5\ \mu\text{l}$) we were able to measure the time between immersion and this audible transition accurately, which we hereafter refer to as the boiling time t_{boil} . Since the film-boiling regime lasted much longer than the bubble-nucleation regime, t_{boil} gives a good estimate of the total cooling time. Based on measurements of drops plunge-cooled in thermocouples (Teng & Moffat, 1998), we estimate that the boiling time is roughly twice the time to cool from room temperature to water’s glass transition temperature, $T_g \simeq 140\text{ K}$.

The drop opacity/transparency was ascertained by optical observation through a stereomicroscope (StereoZoom 6, Bausch and Lomb, Rochester, NY, USA) with fiber-optic illumination (Schott-Fostec, Auburn, NY, USA). To facilitate observations, the solidified drop was raised to just below the LN_2 surface, and a black paper background inserted behind it to enhance contrast.

2.4. X-ray diffraction measurements

X-ray diffraction was used to confirm that the transparent/opaque transition corresponded to the glass/crystal transition, and to characterize the phase of the smallest samples for which ascertaining transparency was difficult. Samples were flash-cooled in LN_2 and then mounted using CryoTongs (Hampton Research) (to minimize the temperature rise during transfer) in a nitrogen gas cryostream at $T = 100\text{ K}$. X-rays were produced by a Rigaku Rotaflex rotating-anode X-ray generator operating at 50 kV and 100 mA, and detected using a Rigaku R-Axis IV++ detector located 200 mm away. Exposure times were 1 min for 1° oscillations, and yielded a d -spacing resolution of less than $2\ \text{\AA}$. Raw X-ray images corresponding to amorphous or polycrystalline states of the solidified drops were analyzed using *HKL2000* (Otwinowski & Minor, 1997) and *Datasqueeze* (Datasqueeze Software, University of Pennsylvania, PA, USA).

Diffraction patterns were acquired for glycerol–water mixtures with drop volumes of 100 nl (in 0.5 mm CryoLoops) and 200 pl (in 100 μm MicroMounts.) The first glycerol

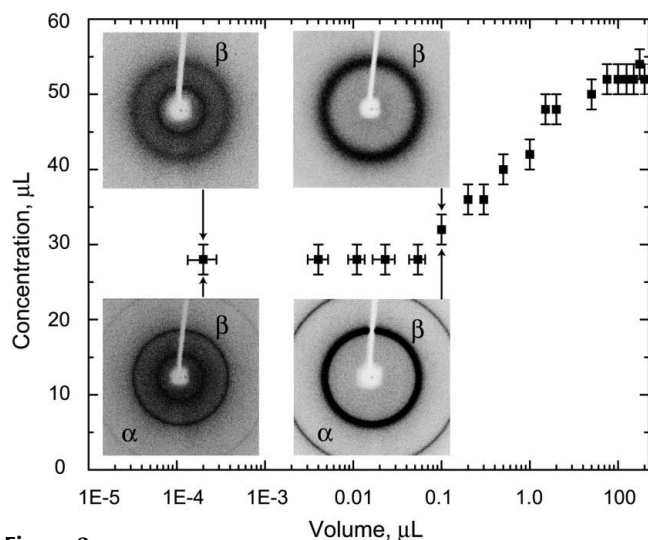


Figure 2
X-ray diffraction images above and below the critical concentration of glycerol. The images on the left are from a 200 pl volume in a 100 μm MicroMount. The images on the right are from a 100 nl volume in a 0.5 mm Hampton CryoLoop. The rings marked α and β are located at 2.24 \AA and 3.70 \AA , respectively. The innermost ring spanning 6.5 \AA to 8.0 \AA in the 200 pl images is from the MicroMount, and is visible because of the very small sample volume and area within the much larger area of the X-ray beam.

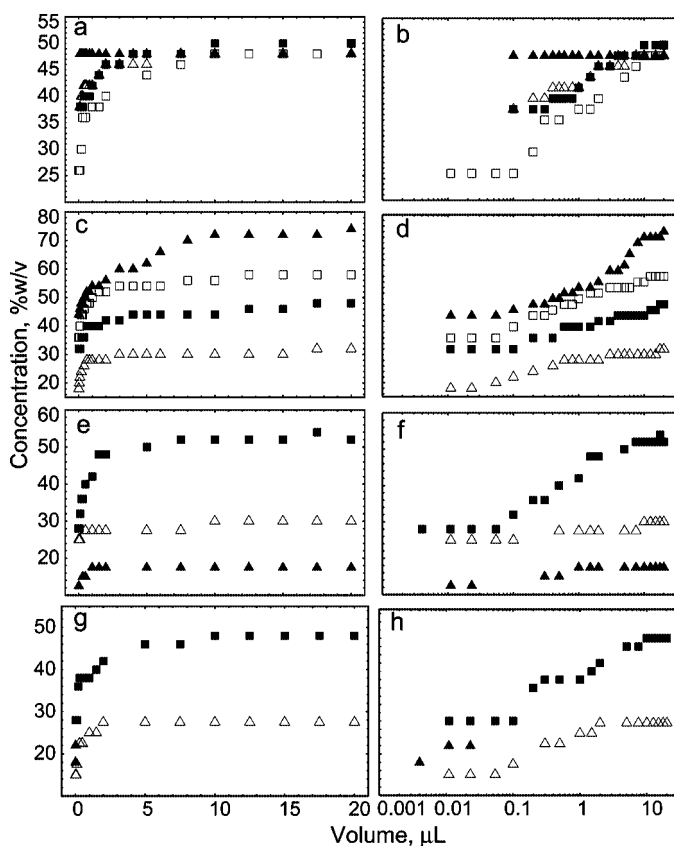


Figure 3
Linear and semi-logarithmic plots of the critical concentration for vitreous ice formation for 14 cryoprotectants. Closed squares represent: PEG200 (*a, b*), xylitol (*c, d*), glycerol (*e, f*), and DMSO (*g, h*); open squares represent: ethylene glycol (*a, b*) and sucrose (*c, d*); closed triangles represent: PEG 20000 (*a, b*), trehalose (*c, d*), 2-propanol (*e, f*), and NaCl (*g, h*); open triangles represent: PEG 2000 (*a, b*), dextrose (*c, d*), methanol (*e, f*), and MPD (*g, h*).

concentration tested was deep in the opaque regime (22% *w/v* for 200 pl and 16% *w/v* for 100 nl), and the concentration was then increased in 2% *w/v* increments through the critical concentration and into the transparent regime (30% *w/v* for 200 pl, and 58% *w/v* for 100 nl). Fig. 2 shows typical diffraction-image sequences at 100 nl and 200 pl, respectively.

3. Results

3.1. Vitreous/polycrystalline phase diagrams and critical CPA concentrations

Visual observation in a microscope proved to be an efficient and reliable way to identify the vitreous-to-polycrystalline ice transition. As shown in Fig. 1, the transition from transparent to opaque drops was dramatic and occurred without an intermediate 'cloudy' phase. For a given CPA and drops of the same volume, the drop-to-drop variation in CPA concentration at the transition was less than 4% *w/v*, and variations presumably reflected differences in drop shape and/or the details of how it cooled.

For larger drops held in wire loops, as the CPA concentration was decreased through the transition region, a patch of opaque ice first formed in the region farthest from the wire, while the rest of the drop remained transparent. This indicates that heat transfer through the wire was more efficient than directly from drop to nitrogen. The patch grew with decreasing CPA concentration until it consumed the entire drop. The critical CPA concentration was determined as the smallest concentration that did not yield a repeatable patch of opaque ice. Similar behavior was not observed for smaller drops mounted in CryoLoops or MicroMounts.

Fig. 3 shows the resulting data for the critical CPA concentration required for vitrification *versus* drop volume, for volumes ranging from ~ 3 nl to ~ 30 μl . The 14 CPAs are grouped into five categories: alcohols (glycerol, methanol, 2-propanol), sugars (sucrose, xylitol, dextrose, trehalose), PEGs (ethylene glycol, PEG 200, PEG 2000, PEG 20000), glycols (DMSO, MPD), and salt (NaCl). Concentrations at and above the indicated critical concentrations yielded transparent vitreous drops, while concentrations below yielded opaque polycrystalline drops.

Most of the studied cryoprotectants show three regimes of behavior: a large-volume (>10 μl) region where the critical concentration is nearly constant; an intermediate-volume region where the critical concentration decreases with decreasing volume; and a small-volume (<0.1 μl) region where the critical concentration again becomes nearly constant. Table 2 gives the critical concentration of each CPA *versus* sample volume, and the ratio of the critical concentrations in the large- and small-volume regimes, respectively.

For NaCl, the solubility limit was reached before vitrification could be achieved at larger volumes. NaCl is a particularly poor cryoprotectant, because it is effective only at small volumes and even then at concentrations that are inhospitable to most proteins and cells. For the PEGs, increasing the molecular weight extended the large-volume region of nearly

Table 2

Minimum cryoprotective agent concentrations (in units of % w/v) for vitrification of 14 CPAs *versus* volume.

Values in units of % v/v can be obtained by dividing % w/v by the CPA density ρ_{CPA} at $T \approx 295$ K listed in the bottom row, obtained from the material safety data sheets. For a given volume, drops flash-cooled with CPA concentrations smaller than those listed yield crystalline ice. If no concentration is listed, then the saturation limit was reached before vitrification could be achieved. The ratio of minimum concentrations at the largest and smallest volumes is listed in the last row. Gly = glycerol, Meth = methanol, Isop = 2-propanol, Sucr = sucrose, Xyl = xylitol, Dext = dextrose, Treh = trehalose, and Eth Gly = ethylene glycol.

V (μ l)	Gly	Meth	Isop	DMSO	MPD	NaCl	Sucr	Xyl	Dext	Treh	Eth Gly	PEG 200	PEG 2000	PEG 20000
20	52	30	17.5	48	27.5		58	48	32	74	50	50	48	48
15	52	30	17.5	48	27.5		58	46	30	72	48	50	48	48
10	52	30	17.5	48	27.5		56	44	30	72	48	50	48	48
7.5	52	27.5	17.5	46	27.5				30		46	48	48	48
5.0	50	27.5	17.5	46	27.5		54	44	30	62	44	48	46	48
2.0	48	27.5	17.5	42	27.5			42	28	56	40	46	46	48
1.5	48	27.5	17.5	40	25		52	40	28	54	38	44	44	48
1.0	42	27.5	17.5	38	25		50	40	28	54	38	42	42	48
0.5	40	27.5	15	38	22.5					50	36	40	42	48
0.4	38	25	15	38	22.5		46	36	26	50	36	40	42	48
0.3	36	25	15	38	22.5		44			48	36	38	40	48
0.2	36	25	15	36	17.5		44	36	24	48	30	38	40	48
0.1	32	25	15	28	17.5		40	32	22	46	26	38	38	48
0.050	28	25	15	28	15		36	32	20	44	26			
0.025	28	25	12.5	28	15	22	36	32	18	44	26			
0.010	28	25	12.5	28	15	22	36	32	18	44	26			
0.005	28	25	12.5	28	15	18								
0.0002	28													
Ratio	1.86	1.20	1.40	1.71	1.83	1.22	1.61	1.5	1.78	1.68	1.92	1.32	1.26	1.00
ρ_{CPA} ($g\ cm^{-3}$)	1.26	0.792	0.785	1.1	0.93	2.16	1.59	1.52	1.54	1.53	1.12	1.12	1.2	1.2

constant critical concentration to lower volumes, and PEG 20000 did not show any volume dependence between 0.1 μ l and 20 μ l.

3.2. Characterization of the vitreous ice/polycrystalline ice transition by X-ray diffraction

X-ray diffraction was used to verify that the transparent–opaque optical transition indeed corresponds with the vitreous ice–polycrystalline ice transition. Vitreous ice (Dowell & Rinfret, 1960) produces a diffuse ring of scattering near 3.7 Å, corresponding to the mean intermolecular spacing in the vitreous phase. Polycrystalline hexagonal ice produces a sharp ring at 2.24 Å (110) and a cluster of three rings [(100), (002) and (101)] with the central ring at 3.7 Å (Dowell & Rinfret, 1960; Murray *et al.*, 2005; Kohl *et al.*, 2000). In the following we refer to the rings at 2.24 and 3.7 Å as α and β rings, respectively. The (220) planes of cubic ice produce a ring at 2.24 Å, and the (111) planes produce one strong ring (as opposed to three rings) at 3.7 Å. The number of rings at the β -ring spacing can thus be used to distinguish the crystalline symmetry of the ice, provided that finite-size broadening determined by the crystallite sizes is smaller than the hexagonal ring spacing.

In previous studies, X-ray diffraction measurements of the vitreous–polycrystalline transition used relatively large (0.1–1 μ l) and ill-defined drop volumes (Garman & Mitchell, 1996; McFerrin & Snell, 2002; Chinte *et al.*, 2005). We examined smaller volumes of 100 nl and 200 pl, which correspond to the range of volumes relevant to protein crystallography on \sim 30–300 μ m crystals.

Figs. 2 and 4 show a subset of a series of diffraction patterns obtained as the glycerol concentration was increased from zero and through the optically determined critical concentration. For both 100 nl and 200 pl volumes, the diffraction patterns of pure water showed scattered spots at the α and β d spacings of hexagonal ice, indicating the presence of a finite

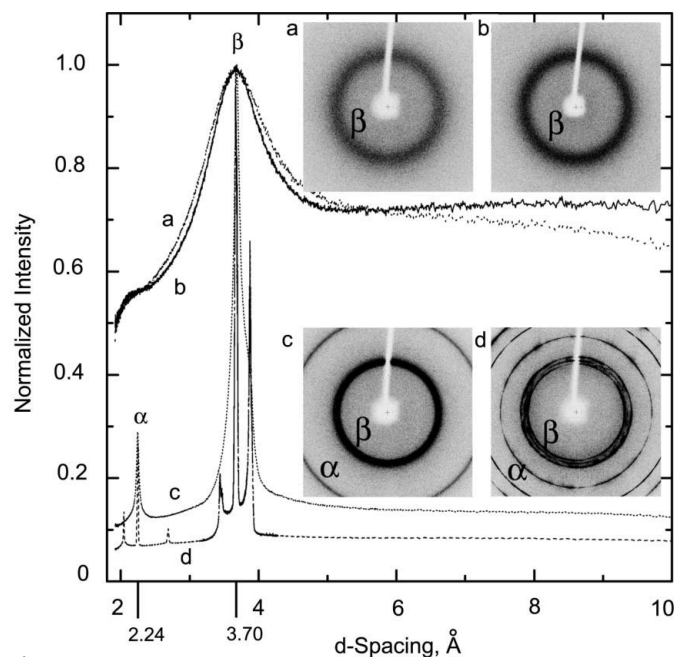


Figure 4 Normalized X-ray diffraction intensity *versus* d spacing of 100 nl flash-cooled drops containing glycerol concentrations of (a) 58% w/v, (b) 32% w/v, (c) 30% w/v, and (d) 16% w/v. Curve a corresponds to the vitreous (transparent) phase; curve b is close to vitreous ice–crystalline ice transition; curve c corresponds to cubic ice or a cubic ice–vitreous ice mixture; and curve d corresponds to hexagonal ice.

number of relatively large crystallites. When glycerol is added, these spots become more numerous and eventually broaden into continuous rings, indicating an increase in the number of randomly oriented hexagonal crystallites and thus a decrease in their size. On further concentration increase, the three hexagonal β rings are replaced by a single, much more intense ring (inset *c*), indicating a phase change from hexagonal to cubic ice (Dowell & Rinfret, 1960; Murray *et al.*, 2005; Kohl *et al.*, 2000). Above a critical glycerol concentration, the α ring disappears and the β ring becomes broad and diffuse (insets *b* and *a*), indicating a transition to vitreous ice.

3.3. Cooling rate measurements

Fig. 5 shows the boiling time, t_{boil} , versus drop volume, V , for a 40% *w/v* glycerol solution, where t_{boil} was determined as the time after a drop was submerged that the audible (and visual) transition from film boiling to nucleate boiling was observed, as discussed in §2.3. For moderate volumes, the data are well described by $t_{\text{boil}} \propto V^{1/2}$ (indicated by the solid line *a*), and for large volumes by $t_{\text{boil}} \propto V^{2/3}$ (indicated by the solid line *b*). Open circles show previous data obtained by directly measuring the cooling time t_c of 0.2 and 0.8 μL drops using a thermocouple (Teng & Moffat, 1998). They are in good agreement with our data, confirming the validity of our measurements even at the shortest cooling times we measured.

4. Discussion

4.1. Behavior versus concentration near the critical concentration

The simple method of optical observation (McFerrin & Snell, 2002) proved remarkably effective for vitreous/polycrystalline phase identification of CPA solutions over the four-orders-of-magnitude volume range explored. This method gives an upper bound on the width of the transition region between polycrystalline and vitreous phases of <4% *w/v*. X-ray measurements on 100 nl glycerol-containing drops further narrow the span of this transition region to less than 2% *w/v*, corresponding to $\sim 6\%$ of the 32% critical concentration. The number of water molecules per glycerol molecule thus changes from 11.7 at the resolved upper concentration limit of the polycrystalline phase to 10.8 at the resolved lower limit of the vitreous phase, for the cooling rate achieved in the 100 nl drop.

4.2. Evolution of ice structure with cryoprotectant concentration

The cubic crystalline form of ice is not observed during slow cooling of water or water–glycerol solutions. For pure water, cubic ice is formed by warming vitreous ice above water's glass transition temperature, T_g . Usually, cubic ice then converts to hexagonal ice at a higher temperature, so there is a thermotropic (temperature-dependent) cubic-to-hexagonal transition (Dowell & Rinfret, 1960; Murray *et al.*, 2005). In our experiments, we observe a robust lyotropic (concentration-depend)

dent) cubic-to-hexagonal transition, controlled by the glycerol concentration. For both the 200 pl and 100 nl drops, the cubic phase is achieved on flash-cooling over a wide glycerol concentration range, suggesting that the cubic ice phase is kinetically favored during flash-cooling and/or that the presence of glycerol modifies the preferred equilibrium ice structure. A similar transition sequence from vitreous to cubic-to-hexagonal ice during flash-cooling has been observed as a function of sucrose concentration (Lepault *et al.*, 1997).

4.3. Volume dependence of the critical CPA concentrations

For most CPAs in Fig. 3, the measured variation of the critical concentration C separating vitreous and polycrystalline phases with drop volume shows three regimes. At large volumes and thus slow cooling rates, the critical concentration for all CPAs is nearly constant. This is consistent with $C \rightarrow C_m$ (Rasmussen & Luyet, 1970; Fahy *et al.*, 1984), where C_m is the minimum CPA concentration for which homogeneous crystal nucleation is completely inhibited and the liquid phase cools directly into the vitreous phase, regardless of cooling rate.

At intermediate volumes, the critical CPA concentration shows a sharp decrease with decreasing volume. The cooling rate increases with decreasing volume, which reduces the time during which nucleation and growth of crystalline ice can occur. For a given CPA concentration, the vitreous phase is kinetically favored beyond a critical cooling rate. Recent measurements (Chinte *et al.*, 2005) on mixtures of glycerol and crystal screen solutions placed in three sizes of CryoLoops (of decreasing but ill-defined volume) show a similar trend of decreasing critical glycerol concentration with decreasing volume. An important exception to this general behavior is provided by higher molecular weight PEGs, which show little or no decrease in concentration with volume. The large volume/slow cooling rate critical concentration C_m in mg ml^{-1}

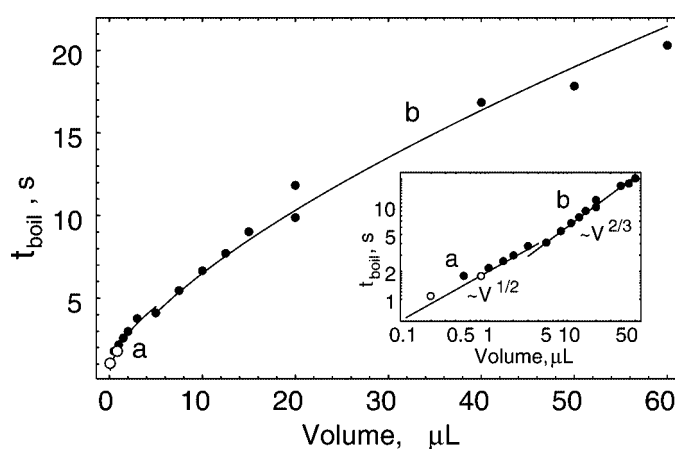


Figure 5

Boiling time versus drop volume for pure water plunged in liquid nitrogen on linear and (inset) log–log scales. Each point (solid circles) represents the average of three independent measurements, with an average residual of ~ 0.16 s. Open circles correspond to data from Teng & Moffat (1998) for 0.2 and 0.8 μL drops plunge-cooled in liquid nitrogen. The fit *a* to data at moderate volumes corresponds to $t_{\text{boil}} \approx V^{1/2}$, and the fit *b* to data at large volumes corresponds to $t_{\text{boil}} \approx V^{2/3}$.

(approximately equivalent to monomers per unit volume) is roughly the same for the various chain lengths, but the shorter chains are more effective in suppressing ice formation at smaller volumes/larger cooling rates. This latter trend is consistent with Garman's observation for $\sim 0.2\text{--}1\ \mu\text{l}$ drops that smaller molecular weight PEGs are more effective cryoprotectants (Garman & Mitchell, 1996).

However, for small volumes ($<0.1\ \mu\text{l}$) the critical concentration levels off and saturates, contrary to naive expectations that smaller volumes should cool faster. This saturation could result either because (i) the cooling rate saturates, or (ii) because a minimum amount of cryoprotectant is required to prevent crystalline ice formation, regardless of the cooling rate.

The second of these hypotheses is inconsistent with experiments showing that pure water can be vitrified if cooling rates are large enough (drop volumes are small enough) (Angell, 2002). As will be discussed elsewhere, to test the first of these hypotheses, CPA-containing drops were sprayed onto the bottom of small cups made from ultra-thin copper foil, which were then immersed in liquid nitrogen. Heat transfer from the drop then occurs primarily *via* its contact with the copper rather than *via* nitrogen vapor or liquid. For volumes of $0.1\text{--}10\ \mu\text{l}$, the critical CPA concentrations measured in this way are a few percent lower than those in Fig. 3, but show the same decrease with decreasing drop volume. However, unlike for drops directly plunged into liquid nitrogen, no plateau is observed at small volumes. Instead, the behavior observed at intermediate volumes continues to the smallest drops (1 pl) measured. This suggests that a saturation in cooling rate is responsible for the small-volume plateau in Fig. 3.

4.4. Critical concentration and critical cooling rate glass/crystal diagram

The measurements of the boiling time in Fig. 5 can be used to determine the cooling rate as a function of drop volume. We define an average cooling rate q as $q = \Delta T/t_c$, where $\Delta T =$

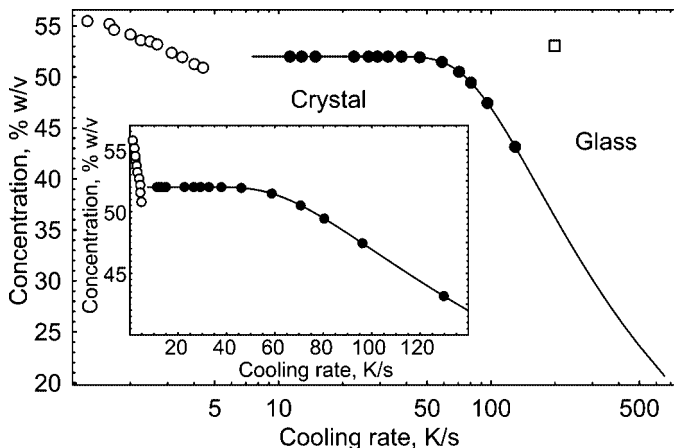


Figure 6 Critical concentration *versus* cooling rate for glycerol on semilog and (inset) linear scales. Solid circles are from the present measurements, and open circles and boxes are from DSC measurements of Sutton (1991a,b) and Kresin & Korber (1991). The solid line is a guide to the eye.

$295 - 77 = 218\ \text{K}$ and t_c is the time to cool to $T = 77\ \text{K}$. Assuming $t_c \simeq t_{\text{boil}}$ and noting that ΔT in our experiments is constant, Fig. 5 corresponds to a plot of the reciprocal cooling rate $q^{-1}(V)$.

By combining $q(V)$ obtained from Fig. 5 with the critical concentration $C(V)$ from Fig. 3, we can eliminate the volume V and obtain the minimum cryoprotectant concentration to achieve vitrification as a function of cooling rate, $C(q)$. This is the function of greatest intrinsic physical interest: $C(V)$ depends on the cooling method (gas stream *versus* liquid plunge) and medium (nitrogen, propane, ethane or helium), whereas $C(q)$ is nominally independent of these parameters and directly connects to the microscopic kinetics responsible for glass formation. It can be used to determine the critical concentration for any cooling method, medium or sample volume. To obtain this function, we use the fits $t_{\text{boil}} \simeq V^{1/2}$ for $0 < V < 5\ \mu\text{l}$ and $t_{\text{boil}} \simeq V^{2/3}$ for $5 < V < 100\ \mu\text{l}$ in Fig. 5, and $C \simeq C_m[1 - \exp(-Va)]^b$ for $C(V)$ in Fig. 3. We exclude data from the small-volume saturation region.

This experimentally determined function for glycerol is shown in Fig. 6. The black circles represent our data and the solid line is a guide to the eye. Below the line, the cooling rate and cryoprotectant concentration are too small to eliminate homogeneous nucleation of crystal ice, and above this line vitreous ice is obtained.

Fig. 6 also shows previous data for the critical cooling rates for water–glycerol mixtures reported by Sutton (1991a,b), indicated by the open circles, and by Kresin & Korber (1991), indicated by the open box. These data were obtained by DSC using surfactant-containing emulsions of glycerol–water drops. Sutton's data in the low-cooling-rate high-concentration region show an increase in critical concentration with decreasing cooling rate, in contrast to the clear plateau evident in our results. This discrepancy may be due to the surfactant, which may affect nucleation. On the other hand, Kresin & Korber's single data point at high cooling rates lies well above our data, suggesting either that the cooling rates actually achieved in their experiment were much lower than reported, or that assumptions in modeling the fraction of crystalline ice present within the vitreous phase were incorrect.

4.5. Comparison with previous work

The basic methods used in the present work, namely X-ray diffraction measurements (Garman & Mitchell, 1996; McFerrin & Snell, 2002; Chinte *et al.*, 2005) and visual observations (McFerrin & Snell, 2002), have been used in previous studies of the effects of CPAs on vitrification of cryoprotective solutions used in protein crystallography. Garman & Mitchell (1996) determined glycerol concentrations required to vitrify 50 crystallization solutions from Hampton Research in a nitrogen cryostream at $T = 100\ \text{K}$. Drops were mounted in single-size ($\sim 1\ \text{mm}$) mohair loops, and their volumes, although not reported, are estimated to be $\sim 0.2\text{--}0.6\ \mu\text{l}$. McFerrin & Snell (2002) extended Garman & Mitchell's experiments to determine critical concentrations of four CPAs (glycerol, PEG 400, ethylene glycol and propylene glycol)

required to vitrify 98 different crystallization solutions from Hampton Research, using 0.7–1 mm CryoLoops and nitrogen cryostream cooling. The critical concentrations determined for the single volume examined in both these studies for drops containing a single cryoprotectant are consistent with the present results, although the present results provide better resolution (2% *w/v* versus 6% *w/v*). Recently, Chinte *et al.* (2005) used CryoLoops of sizes of 1, 0.5 and 0.1 mm to determine critical glycerol conditions in a $T = 100$ K nitrogen cryostream, for 12 different crystallization solutions from Hampton Research. Sample volumes were not measured, but the expected decrease in critical glycerol concentration with loop size was observed.

5. Conclusion

We have described the first quantitative and systematic measurements of critical cryoprotectant concentrations for plunge-cooling in liquid nitrogen in the volume range relevant to cryocrystallography and to the cryopreservation of small numbers of cells. For most of the fourteen CPAs examined, the critical CPA concentration is constant at large volumes, decreases strongly with decreasing volume for intermediate volumes, and then has a plateau at small volumes. We have combined these measurements of critical concentration *versus* volume with measurements of cooling times *versus* volume to obtain the quantity of greatest intrinsic physical interest in flash-cooling: the minimum CPA concentration for vitrification *versus* cooling rate. Our results can be used to develop more rational approaches to cryopreservation of protein crystals and other biological samples. They also provide a starting point for understanding the physics of flash-cooling and vitrification of aqueous cryoprotectant mixtures.

The authors would like to thank Dr Jan Kmetko, Eugene Kalinin and Dr Angela Toms for their assistance in operating the X-ray diffractometer and in interpreting the resulting images. This work was funded by the National Institute of Health (R01 GM65981).

References

- Angell, C. A. (2002). *Chem. Rev.* **102**, 2627–2650.
- Chayen, N. E., Boggon, T. J., Cassetta, A., Deacon, A., Gleichmann, T., Habash, J., Harrop, S. J., Helliwell, J. R., Nieh, Y. P., Peterson, M. R., Raftery, J., Snell, E. H., Hadener, A., Niemann, A. C., Siddons, D. P., Stojanoff, V., Thompson, A. W., Ursby, T. & Wulff, M. (1996). *Quart. Rev. Biophys.* **29**, 227–278.
- Chinte, U., Shah, B., DeWitt, K., Kirschbaum, K., Pinkerton, A. A. & Schall, C. (2005). *J. Appl. Cryst.* **38**, 412–419.
- Dowell, L. G. & Rinfret, A. P. (1960). *Nature (London)*, **188**, 1144–1148.
- Fahy, G. M., MacFarlane, D. R., Angell, C. A. & Meryman, H. T. (1984). *Cryobiology*, **21**, 407–426.
- Garman, E. (1999). *Acta Cryst.* **D55**, 1641–1653.
- Garman, E. F. & Mitchell, E. P. (1996). *J. Appl. Cryst.* **29**, 584–587.
- Garman, E. F. & Schneider, T. R. (1997). *J. Appl. Cryst.* **30**, 211–237.
- Hope, H. (1990). *Annu. Rev. Biophys. Biophys. Chem.* **19**, 107–126.
- Incropera, F. P. & De Witt, D. P. (1981). *Fundamentals of Heat and Mass Transfer*. New York: John Wiley.
- Juers, D. H. & Matthews, B. W. (2004). *Quart. Rev. Biophys.* **37**, 105–119.
- Kresin, M. & Korber, Ch. (1991). *J. Chem. Phys.* **95**, 5249–5255.
- Kohl, I., Mayer, E. & Hallbrucker, A. (2000). *Phys. Chem. Chem. Phys.* **2**, 1579–1586.
- Lepault, J., Bigot, D., Studer, D. & Erk, I. (1997). *J. Microsc.* **187**, 158–166.
- Luyet, B. & Rasmussen, D. (1968). *Biodynamica*, **10**(211), 167–191.
- MacKenzie, A. P. (1977). *Philos. Trans. R. Soc. London B*, **278**, 167–189.
- McFerrin, M. B. & Snell, E. H. (2002). *J. Appl. Cryst.* **35**, 538–545.
- Murray, B. J., Knopf, D. A. & Bertram, A. K. (2005). *Nature (London)*, **34**, 202–205.
- Otwinowski, Z. & Minor, W. (1997). *Methods Enzymol.* **276**, 307–326.
- Rasmussen D. & Luyet B. (1970). *Biodynamica*, **11**(225), 33–44.
- Rodgers, D. W. (1994). *Structure*, **2**, 1135–1140.
- Stralen, A. van & Cole, R. (1979). *Boiling Phenomena*, Vol. 1. New York: Hemisphere.
- Sutton, R. L. (1991a). *J. Chem. Soc. Faraday Trans.* **87**, 101–105.
- Sutton, R. L. (1991b). *J. Chem. Soc. Faraday Trans.* **87**, 3747–3750.
- Teng, T. & Moffat, K. (1998). *J. Appl. Cryst.* **31**, 252–257.
- Thorne, R. E., Stum, Z., Kmetko, J., O'Neill, K. & Gillilan, R. (2003). *J. Appl. Cryst.* **36**, 1455–1460.
- Turnbull, D. & Fisher, J. C. (1949). *J. Chem. Phys.* **17**, 71.